Applied Clay Science 245 (2023) 107127

Contents lists available at ScienceDirect

Applied Clay Science

journal homepage: www.elsevier.com/locate/clay

Research Paper

Insight and mechanisms of tetracycline adsorption on sodium alginate/montmorillonite composite beads

Po-Hsiang Chang [a,*], Raj Mukhopadhyay [b,c], Binoy Sarkar [d], Yun-Cheng Mei [e], Chih-Hsun Hsu [e], Yu-Min Tzou [e,f,**]

[a] College of Resources and Environment, Fujian Agriculture and Forestry University, Fuzhou 350002, PR China
[b] Division of Irrigation and Drainage Engineering, ICAR-Central Soil Salinity Research Institute, Karnal 132001, Haryana, India
[c] Department of Chemistry, Mellon College of Science, Carnegie Mellon University, Pittsburgh 15213, US
[d] Future Industries Institute, University of South Australia, Mawson Lakes, SA 5095, Australia
[e] Department of Soil and Environmental Sciences, National Chung Hsing University, 145 Xingda Rd., Taichung 40227, Taiwan
[f] Innovation and Development Center of Sustainable Agriculture, National Chung Hsing University, 145 Xingda Rd., Taichung 40227, Taiwan

ARTICLE INFO

Keywords:
Tetracycline
Montmorillonite
Sodium alginate
Cation exchange
Water treatment

ABSTRACT

The presence of antibiotics in soil and water raises great health concerns because they may increase the development of harmful antibiotic-resistant bacteria. In this study, composite beads prepared from 2:1 or 1:1 ratios of montmorillonite (Mt) and sodium alginate (SA) were used to adsorb tetracycline hydrochloride (TC), an antibiotic commonly found in aqueous systems. The equilibrium time for TC adsorption onto the Mt/SA was 8 h, and the kinetic data were consistent with the pseudo-second-order model. The adsorption isotherm was described with the Langmuir equation. The maximum amounts of TC adsorbed were 745, 689, and 445 mg g^{-1} for the 2:1- and 1:1-Mt/SA and the original Mt, respectively. The Mt/SA composite beads exhibited porous structures; however, this did not play a key role in TC removal, as previously reported. Cation exchange was the major adsorption mechanism, and electrostatic attraction and hydrogen bonding between the SA and TC also contributed to TC adsorption on the Mt/SA composite beads. In addition, the migration of a small amount of TC into the inner spaces of the beads led to the intercalation of the TC in the Mt interlayers and enhanced TC adsorption by the Mt/SA composite beads.

1. Introduction

Tetracycline hydrochloride (TC) is a common medicinal drug used to counter the negative impacts of gram-positive and gram-negative bacteria and many protozoan parasites in humans and animals (Roberts, 2002). This antibiotic has been classified as an emerging pollutant and has raised increasing concern over environmental deterioration resulting from widespread use (Sarmah et al., 2006; You et al., 2020). The TC compounds are very difficult to degrade in the natural environment, and therefore, their residues remain in the environment for long periods of time (Peng et al., 2022). The average concentrations of tetracycline determined for groundwater, lake water, wastewater and influent wastewater from pig farms ranged between 7.9 and 1172.3 ng L^{-1} in the summer and 5.8–409.5 ng L^{-1} in the winter (Tong et al., 2009). The seasonal change of water usage in pig farms and difference in environmental conditions (especially the temperature and rainfall) were responsible for the observed concentration variations of the analytes. The rainfall could reduce the TC concentration by dilution with rainwater. The effect of temperature on pollutant degradation in different seasons could be another important factor. Tetracycline residues were found at concentrations of 2.37 ng L^{-1} in the Yangtze River Estuary (Yan et al., 2013). The maximum detected TC concentration was 623.43 ng L^{-1} in the Tiaoxi River of China (Li et al., 2016). Entry of TC into humans through consumption of contaminated drinking water and food (accumulated in the food chain through irrigation water) may cause leptospirosis, amebiasis, and pelvic inflammatory diseases (Daghrir and Drogui, 2013). Conventional water treatment systems such as chlorination, membrane filtration, advanced oxidation, coagulation, and biological treatment are not able to remove low concentrations (ng L^{-1}) of TC from water (Azanu et al., 2018). Adsorption methods are widely

* Corresponding author at: College of Resources and Environment, Fujian Agriculture and Forestry University, Fuzhou 350002, P.R. China
** Corresponding author at: Department of Soil and Environmental Sciences, National Chung Hsing University, 145 Xingda Rd., Taichung 40227, Taiwan.
E-mail addresses: phchang@fafu.edu.cn (P.-H. Chang), ymtzou@dragon.nchu.edu.tw (Y.-M. Tzou).

https://doi.org/10.1016/j.clay.2023.107127
Received 30 May 2023; Received in revised form 2 September 2023; Accepted 3 September 2023

used due to their ease of operation and low costs (Yu et al., 2016). Many adsorbents, such as activated carbon, biochar, single-layer graphene oxide, nanoparticles, and carbon nanotubes, have been developed for TC removal from water (Ashraf et al., 2022; Hu et al., 2022; Zou et al., 2022). When choosing adsorbents, large specific surface areas, well-developed pore structures, functional groups, easy availability, and inexpensive materials must be considered. It is necessary to develop an innovative, efficient, environmentally compatible, easy-to-handle and low-cost adsorbent material to remove TC from water and limit transfer from the water or soil to humans in order to achieve environmental sustainability.

Sodium alginate (SA) is extracted from algae (~21%) and widely used to prepare composite beads that remove contaminants from water because SA is a biodegradable, renewable, economical, and environment friendly material (Mohammed et al., 2020) and is highly soluble in water (Benavides et al., 2012). At room temperature, the addition of divalent cations (such as Ca^{2+}) into SA aqueous solutions results in stable coagulation (Liao et al., 2017). The molecular structure of SA contains many hydroxyl groups (−OH) and carboxyl groups (−COOH), which are active adsorption sites used in removing organic contaminants such as dyes, pesticides, and antibiotics (Zhang et al., 2023). However, the stability of SA is an issue; therefore, it has to be modified by physico-chemical methods, such as introducing inorganic materials into the SA matrix to prepare composite beads and improve their surface specific areas and stabilities, before using it in aqueous systems for the adsorptive removal of contaminants (Gao et al., 2018; Gao et al., 2019).

The preparation of composite beads containing SA as the active substrate previously included a Y-immobilized graphene oxide-alginate hydrogel (He et al., 2020), double-network polyvinyl alcohol-copper alginate gel beads (Liao et al., 2022), Cu-immobilized alginate (Zhang et al., 2019a), phenolic hydroxyl-derived copper alginate (Zhang et al., 2019b), graphene oxide (Gao et al., 2012), magnetic graphene oxide (MGO) (Huang et al., 2019), magnetic chemically reduced graphene (MCRG) (Huang et al., 2019), and magnetic annealing-reduced graphene (MARG) (Huang et al., 2019) exhibiting TC removal capacities of 477.9, 231.4, 53.3, 153.9, 313, 252, 104.5, and 24.2 mg g^{-1}, respectively. However, the preparations of these composite beads were expensive and required complex synthetic procedures, and their use in environmental remediation was limited by the lack of a standard protocol.

Montmorillonite (Mt) clay mineral is inexpensive and widely used for the removal of contaminants from aqueous systems (Zhu et al., 2016). Mt is often introduced in the form of composite beads to enhance the functional capacity and stability of biodegradable polymers such as chitosan and alginate (Hou et al., 2015; Park et al., 2016). Furthermore, atomic models for Mt such as SAz-2 show that the −OH on the surfaces of the aluminosilicates form hydrogen bonds (Liang et al., 2016), which significantly improved the pore architectures of alginate aerogels with numerous hydrogen bonding networks. The present study is designed to prepare and characterize novel Mt/SA composite beads and optimize the proportions of the individual components for efficient removal of TC from water. It was hypothesized that the stability of the Mt/SA composite beads would differ with different Mt-SA ratios and that an optimum ratio for the inorganic and organic components would provide the maximum TC removal capacity of the Mt/SA composite beads, and this has not been studied previously. Furthermore, the formation of suspensions by Mt limits its use in environmental remediation, even though Mt has an astonishing removal capacity. Consequently, the use of composite beads could overcome the barriers to practical application. Under this scenario, batch adsorption isotherms were generated, kinetic studies were performed and various environmental factors (e.g., temperature, ionic strength and pH) affecting TC adsorption were optimized. A mechanistic understanding of TC removal by Mt, by SA alone and by the Mt/SA composite was developed by characterizing the adsorbents with X-ray diffraction (XRD), thermogravimetric analysis (TGA) and Fourier transform infrared (FTIR) spectroscopy.

2. Materials and methods

2.1. Materials

2.1.1. Montmorillonite (SAz-2), SA and TC

The SAz-2 used was a dioctahedral smectite obtained from the Clay Minerals Society of the USA. The reported parameters of SAz-2 are listed in Table S1. The SAz-2 contains 95% of Mt. The TC (tetracycline hydrochloride) used in the study was obtained from Calbiochem (Darmstadt, Germany) with a purity of 98% (CAS: 60–54-8). The physicochemical properties of the TC are given in Fig. S1a, b. The water-soluble nontoxic SA was purchased from Aladdin (Shanghai, China). The SA contained many −OH (Fig. S1c).

2.1.2. Composite bead synthesis

To ensure the quality of the beads, we integrated the granulation steps of previous studies and optimized this step to prepare composite bead solid samples with Mt:SA = 1:1 and 2:1. In the preparation, two 250 mL beakers were filled with 100 mL of deionized water, 2 g of SA was added to each beaker, and the mixtures were stirred with 600 rpm magnetically for several hours until the SA was dissolved. Finally, 2 and 4 g of Mt were added to the beakers and magnetically stirred for 8 h for even mixing. The stirred and mixed gel solution was poured into a 50 mL syringe and used to soak particles dropped into a $CaCl_2$ (4%) solution for 6 h to facilitate shaping. Then, the 4% $CaCl_2$ solution was poured out, the beads were washed three times with deionized water, soaked in deionized water for 3 h to remove the residual $CaCl_2$, and then washed three times with deionized water to obtain raw beads with an average size of 0.3 mm (Fig. S2). Finally, they were heated at 60 °C for 12 h in an oven to obtain composite beads with an average size of 0.1 mm.

2.1.3. Composite beads stability

During the granulation process, we found that the experimental conditions were very important, otherwise, the granulation was found to be unsuccessful. Thus, this process needed attention in several areas. For example, the preparation vessel needs to use a beaker with a large bottom area, otherwise magnetic stirring was not able to uniformly mix the components due to the high viscosity of SA. Secondly, SA should be used with high viscosity because low viscosity SA cannot be granulated with Mt. Third, composite beads will gradually collapse when the pH value of the mixture is >8, and they will not collapse when the pH value is between 2 and 7. Fourth, in actual application of environmental remediation, attention must be paid to the pH value of the solution in order to achieve the beneficial effects of the composite beads.

2.2. Adsorption experiments

All batch experiments were run in duplicate and the amounts of composite beads used was 0.10 g (about 12–13 bead numbers), while the volume of solution used was 20 mL and they were combined in 50 mL centrifuge tubes and mixed on a reciprocal shaker at 150 rpm, room temperature. The TC concentration was at the level of ng L^{-1} or μg L^{-1} in most aquatic environments, however, in order to understand the mechanism of TC adsorption behavior on Mt/alginate beads, observable changes in the physico-chemical properties of adsorbents were required, which were obtained only with a high TC concentration in the batch adsorption system. It is difficult to observe the above changes in a low (environmentally relevant; ng L^{-1}) TC concentration range.

For adsorption kinetic studies, the initial TC concentration was 1500 mg L^{-1}, where the pH values were maintained at 3.0–3.3 without any pH adjustment. The mixtures were shaken for 0.25, 0.5, 1.0, 2.0, 4.0, 8.0, 16.0, and 24.0 h. The effect of pH on TC adsorption was conducted at pH values between 2.0 and 7.0 with a 1-unit increment at an initial TC concentration of 1500 mg L^{-1}. The poor mechanical strength of SA made it unstable to conduct the pH edge experiment above pH 7. For ionic strength experiments, the initial TC concentration was 1500 mg L^{-1},

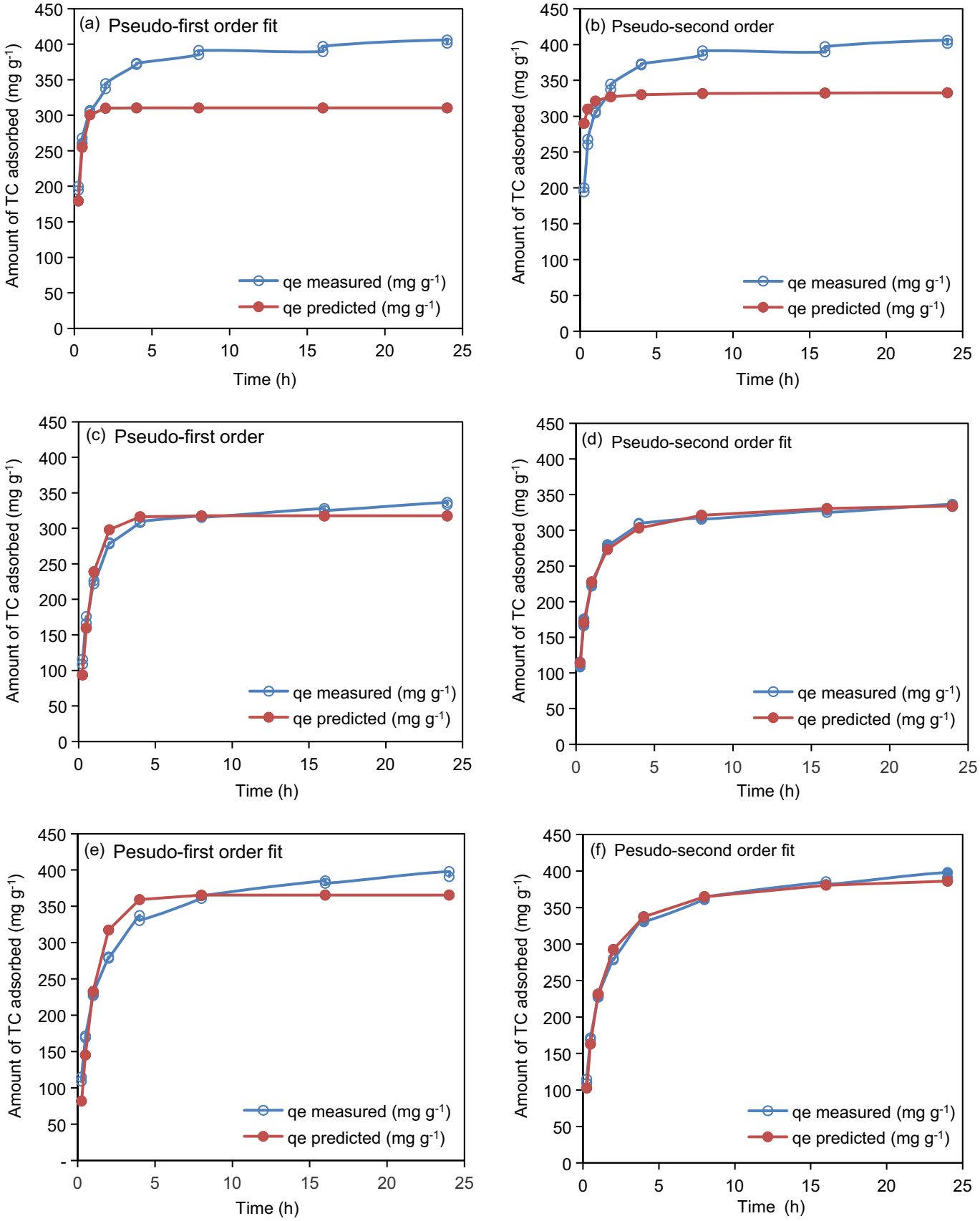

Fig. 1. Adsorption kinetics of TC removal by origin Mt (a, b), 1:1 Mt/SA (c, d), and 2:1 Mt/SA (e, f) for pseudo-first order and pseudo-second order fitting, respectively, under initial concentration of 1500 mg L^{-1}.

Table 1
Estimated kinetic model parameters for TC adsorption onto 2:1, 1: 1 Mt/SA composite beads, original Mt.

Kinetic models	Parameters	2:1 Mt/SA	1:1 Mt/SA	Original Mt
Pseudo-first order	q_e (mg g^{-1})	365.55	317.55	310.25
	k_1 (h^{-1})	1.01	1.39	3.45
	R^2	0.94	0.96	0.27
	R^2_{adj}	0.93	0.96	0.22
	RMSEP	25.36	14.32	60.08
	RPD	4.16	5.66	0.73
Pseudo-second order	q_e (mg g^{-1})	397.66	340.82	333.27
	k_2 (g mg^{-1} h^{-1})	0.0034	0.005	0.080
	R^2	0.99	0.99	0.33
	R^2_{adj}	0.99	0.99	0.28
	RMSEP	7.76	4.77	57.66
	RPD	12.83	15.97	0.24

while the NaCl molarity were at 0.001, 0.01, 0.1 and 1.0 mol L^{-1}, respectively. In temperature dependent adsorption, the temperature was maintained at 298, 313, and 328 K with initial TC concentration 1500 mg L^{-1}. For adsorption isotherm study, the initial concentrations were at 100, 250, 500, 750, 1000, 1500, 2000, 2500, 3000 and 4000 mgL^{-1}, while the pH was maintained between 2.8 and 5.0. Under this pH range, TC acted as a cation (Fig. S1).

The centrifuge tubes were wrapped in aluminum foil to prevent light induced decomposition during mixing and storage processes. After mixing, samples did not require centrifugation to seperate the liquid because the beads quickly settled down by gravity at the bottom of the tubes. The supernatants were passed through a 0.45 μm filter and analyzed for equilibrium TC concentrations using UV/VIS spectroscopy method. A control experiment (You et al., 2020) indicated that no TC degradation or adsorption on centrifuge tubes occurred during the mixing. The amount of TC absorbed was determined by the difference between initial and equilibrium concentrations.

2.3. Instrumental analyses

The equilibrium concentrations of TC were analyzed by a SPECORD 210 PLUS UV/VIS Spectrophotometer (Analytikjena, Hamburg, Germany). The detection wavelength was 254 nm for TC quantification. Calibration was made with 4 standards between 5 and 50 mg L^{-1} with an $R^2 = 0.99$. Some high concentration samples were needed to be diluted before analysis to let the UV/VIS spectroscopy readings <1.0. The concentrations of desorbed ions were detected by Dionex high-pressure ion chromatography (Thermo Fisher Scientific™, Waltham, USA) equipped with a Dionex IonPac™ CS12A-5 μm column (3 × 150 mm). The mobile phase was 20 mmol L^{-1} methanesulfonic acid (1.922 mL in 1 L of water), and the flow rate was maintained at 0.5 mL min^{-1}. The retention times of calcium, magnesium, sodium, and potassium ions were 2.7, 3.78, 5.92 and 7.38 min, respectively. XRD analysis was performed using a PANanalytical X PERT PRO diffractometer (TEXAS Instrument, Texas, USA) equipped with a Cu target radiation, and an X'Celerator detector at a step size of 0.033 and a scanning speed of 5° min^{-1}. The samples were measured at a 4–22° 2θ range under 45 kV and 40 mA. The FTIR analysis was conducted via a KBr pellet suppression method on a NEXUS FTIR spectrometer (Thermo Nicolet, Waltham, USA). The spectra were collected between wavenumber 4000–400 cm^{-1} with 4 cm^{-1} resolution and averaging 256 scans. The TGA was performed under an N_2 environment, with a 10 °C min^{-1} heating rate on a TA-Q500 equipment (TA Instruments, Delaware, USA). A JEOL JSM-7800F (OXFORD Instrument, oxford, UK) field-emission scanning electron microscope (FE-SEM) was used to determine the surface structure of the beads. The microscopic images of composite beads were taken by the Keyence VK-X1000 laser microscope (Analytikjena, Hamburg, Germany). A laser scanning microscopy VK-X1000 (Keyence, Taipei, Taiwan) was used to display the real morphologies of composite beads.

3. Results and discussion

3.1. Kinetics of adsorption

The adsorption kinetic data are displayed in Fig. 1, and the results revealed that a pseudo-second-order model provided the best fit to the experimental data (a detailed discussion of the model equation and fitting parameters is provided in the SI). The coefficient of determination (R^2) was 0.99 for an initial TC concentration of 1500 mg L^{-1} (Table 1) and indicated the possibility of chemical adsorption via chemical bond formation or ion exchange (He et al., 2020; Hu et al., 2019; Liao et al., 2022;). In addition, the TC adsorption equilibrium time was 8 h for both Mt/SA ratios, but the amount adsorbed reached 90% within 4 h (Fig. 1). The equilibrium time for TC adsorption in this study was superior to that reported for an initial TC concentration of 1500 mg L^{-1} (Table S2). An equilibrium adsorption level close to that predicted from the pseudo-second-order model would indicate that chemical adsorption and pore mass transfer might have played pivotal roles in the adsorption process (Chang et al., 2009a). In the first 0.25 h, the amounts of TC adsorbed in our study were 200, 110, and 110 mg g^{-1} for original Mt, 2:1- and 1:1-Mt/SA (Fig. 1), respectively. The TC adsorption capacities for 2:1- and 1:1-Mt/SA ratios were both higher than 110 mg g^{-1} for the kinetic studies, indicating a high affinity between TC and the composite Mt/SA beads. Although the amounts of clay in the composite beads were less than the original amounts, the bead pore structure could have increased the amounts adsorbed. Therefore, the increase in the amount of TC adsorbed was likely due to co-adsorption involving the pore spaces and cation exchange. The higher adsorption capacities were observed in the kinetic adsorption experiments, especially for the 2:1 beads (Fig. 1). In summary, the results showed that the 2:1- and 1:1-composite beads displayed equilibrium times similar to that of the original Mt powder.

The kinetic model showed that the amount of TC adsorbed reached a maximum after 24 h. Therefore, subsequent isothermal studies were conducted over an equilibration time of 24 h.

3.2. Adsorption isotherms

The Freundlich and Langmuir isotherms for adsorption of TC on the 2:1- and 1:1-composite beads at pH 2.8–5.0 are plotted in Fig. 2. The experimental data was well fitted with the Langmuir isotherm. The maximum potential adsorption capacities were 745, 689, and 445 mg g^{-1} for the 2:1, 1:1 ratios and original Mt, respectively (Table 2). The 2:1- and 1:1-composite beads showed better TC adsorption capacities of 745 and 689 mg g^{-1} compared to a cation exchange capacity of 123 $cmol_{(+)}$ kg^{-1} for original Mt (SAz-2). Additionally, these 2:1- and 1:1-composite beads both exhibited higher adsorption capacities compared to those of many previous studies (Table S3). The original Mt exhibited a TC adsorption capacity (445 mg g^{-1}) similar to that reported earlier (Chang et al., 2009a). Interestingly, the amounts of Mt in the 2:1- and 1:1-beads were less than the original amount of Mt. Therefore, if adsorption occurred via a cation exchange mechanism, the amount of TC adsorbed would decrease with decreasing amounts of Mt in the different Mt/SA ratios. However, the adsorption capacities of the 2:1- and 1:1-beads were greater than that of the original Mt (Fig. 2). In addition, the best R^2 value was found for the Langmuir model (Table 2), which indicated monolayer adsorption, as reported in previous studies of TC adsorption (Liao et al., 2022; Zhang et al., 2019b), instead of the Freundlich model (He et al., 2020; Huang et al., 2019; Zhang et al., 2019b). Furthermore, we were able to determine the separation factor for the Langmuir isotherm model (Zhang et al., 2019b).

The value of R_L indicated the thermodynamic behavior of the isotherms. When $R_L = 0$, $0 < R_L < 1$, $R_L = 1$, and $R_L > 1$ corresponded to irreversible, favorable, linear, and unfavorable, respectively (Li and Zhang, 2010). The value of R_L (Fig. S3) ranged from 0.18 to 0.92, indicating favorable adsorption of TC on the 2:1- and 1:1-beads. Therefore, the higher amounts of TC adsorbed on the 2:1- and 1:1-

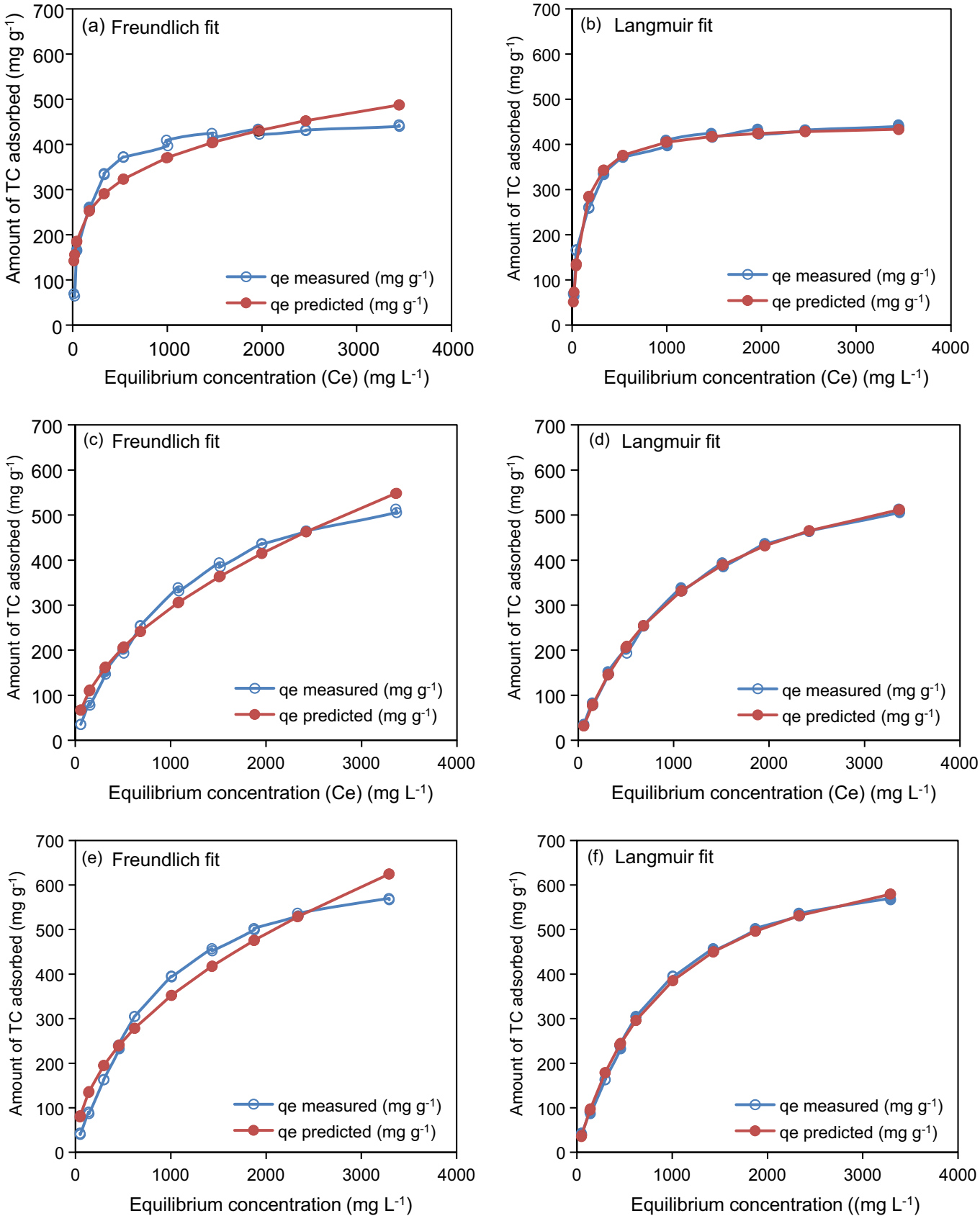

Fig. 2. Adsorption isotherms of TC sorption on original Mt (a, b), 1:1 Mt/SA (c, d), and 2:1 Mt/SA (e, f) for Freundlich and Langmuir fitting, respectively, at pH 2.8–5.0.

Table 2
Estimated isothermal model parameters for TC adsorption onto 2:1, 1: 1 Mt/SA composite beads, original Mt.

Isothermal models	Parameters	2:1 Mt/SA	1:1 Mt/SA	Original Mt
Freundlich	K_f (mg g^{-1})	12.42	8.44	80.9
	1/n (L g^{-1})	0.48	0.51	0.2
	R^2	0.96	0.98	0.89
	R^2_{adj}	0.95	0.97	0.89
	RMSEP	36.34	24.93	40.09
	RPD	4.64	6.02	2.69
Langmuir	b (L mg^{-1})	0.001	0.0008	0.010
	q_m (mg g^{-1})	745.0	689.5	445.6
	R^2	0.99	0.99	0.98
	R^2_{adj}	0.99	0.99	0.98
	RMSEP	9.14	5.45	15.19
	RPD	19.57	29.07	8.25

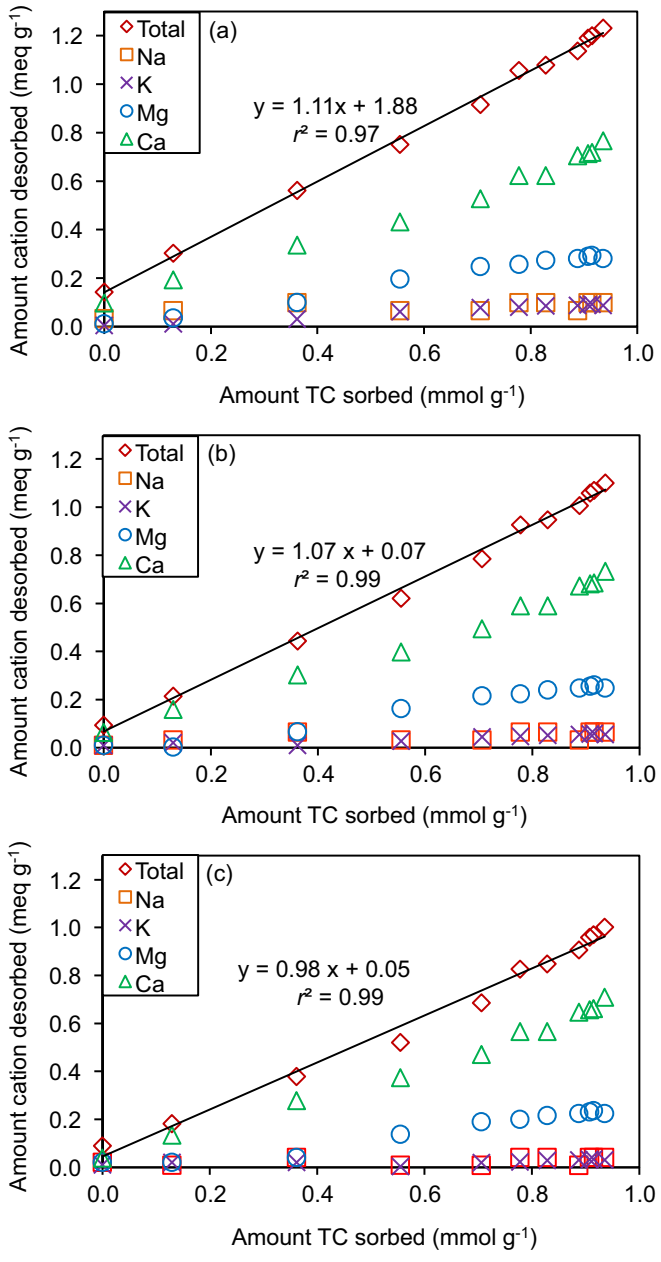

Fig. 3. Amounts of desorbed metal cations from original Mt (a),1:1 Mt/SA (b), and 2:1 Mt/SA (c) as affected by the amount of TC adsorption.

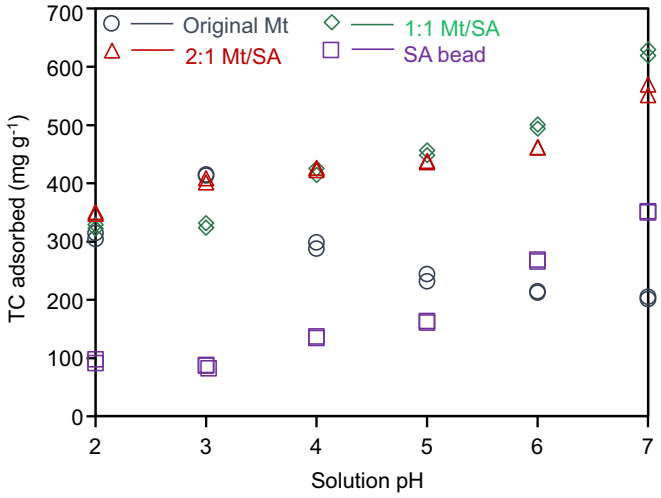

Fig. 4. TC uptake on original Mt, 1:1 Mt/SA, 2:1 Mt/SA, and SA bead as affected by equilibrium solution pH at initial concentration of 1500 mg L^{-1} at 298 K.

beads were likely due to the pore structures. This was observed from the ocular sign images of breaking beads (Fig. S4). Indeed, the SA beads contributed approximately 160 mg g^{-1} TC to the adsorption levels (Fig. S5), and this may have involved electrostatic interactions between the hydroxyl groups of the SA and the cationic TC within the pH range 3–5. However, the SA beads contained 100% SA, which was higher than the proportions in the 2:1- and 1:1-beads; thus, the actual amounts of SA adsorbed inside the 2:1- and 1:1-beads should be <160 mg g^{-1}. Nevertheless, the SA beads showed higher amounts of cationic compounds or ions adsorbed on the composite beads made with SA-based materials. This is a significant result that many previous studies did not discuss.

Previous studies using energy dispersive spectroscopy (EDS) showed that the Na^+ in the interlayers of Na-montmorillonite were removed by bead formation (Das et al., 2021; Fernandes et al., 2018). Thus, the interlayers were saturated with the SA (Das et al., 2021). However, we observed a different result for SAz-2 (Ca-montmorillonite) in this study. The desorption of metal cations and the sorption of TC displayed a positive correlation (Fig. 3). The amounts of K^+ and Na^+ released were low and almost unaffected by the amount of TC adsorbed. However, the amount of Mg^{2+} released was slightly higher due to the 6.46% MgO content in the original Mt (Table S1). The principal cation desorbed was Ca^{2+}, and the amount of Ca^{2+} desorbed was much higher than the amount of TC adsorbed; this indicated that cation exchange was involved in TC adsorption, as reported previously (Chang et al., 2009a, 2009b; Chang et al., 2019). Similarly, the TC adsorption was higher at low pH and under low Ca^{2+} concentration which corroborated with our results indicating that desorbed Ca^{2+} was much higher which facilitated the TC adsorption (Aristilde et al., 2016; Parolo et al., 2012). However, the material used in this study was combined with Mt and SA, and the Mt continued the cation exchange process, but the SA did not. The maximum capacity of TC adsorbed on 0.1 g of SA was 160 mg g^{-1}, and the amounts adsorbed on the 2:1- and 1:1-beads should be less than that for 0.1 g of SA. Therefore, the influence of SA on the adsorption capacities of the 2:1- and 1:1-beads was not significant. Thus, the slope of these curves (Fig. 3) still suggested that cation exchange was the main adsorption mechanism based on the values of 0.98, 1.07, and 1.11 for the original, 1:1, and 2:1 samples, respectively (Fig. 3). The cations desorbed from the 2:1- and 1:1-beads could have been replaced by H^+ because the pH of the medium was between 3 and 5 (Chang et al., 2009b; Chang et al., 2019; Figueroa et al., 2004). The positive correlation between the amounts of TC adsorbed and the cations desorbed implied that cation exchange played a significant role in TC adsorption

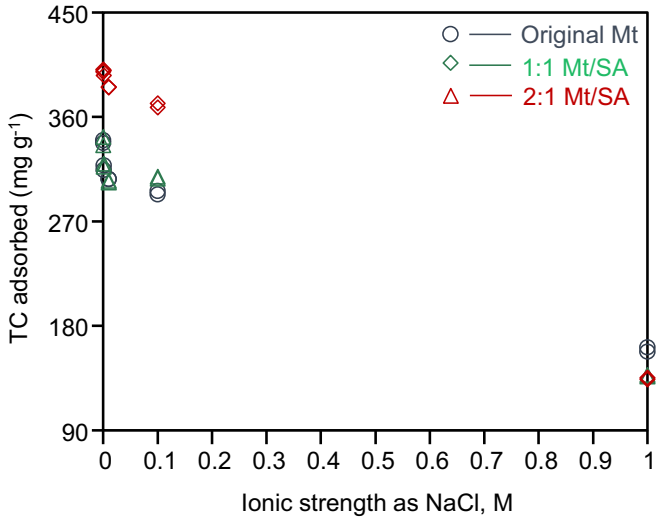

Fig. 5. TC uptake on original Mt, 1:1 Mt/SA, and 2:1 Mt/SA, as affected by ionic strength under initial concentration of 1500 mg L^{-1}.

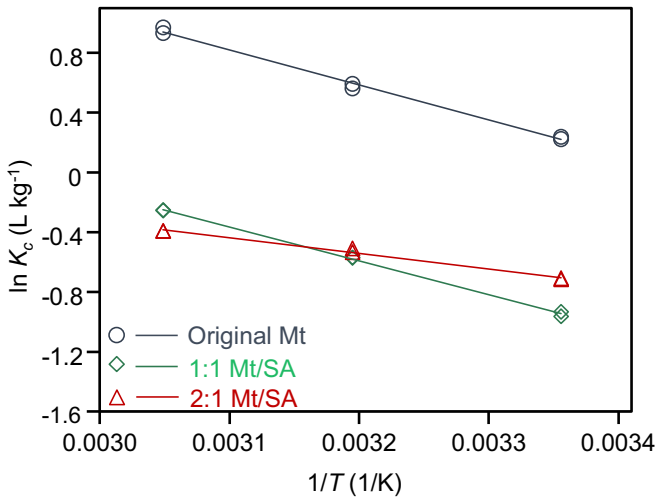

Fig. 6. TC removal by original Mt, 1:1 Mt/SA, and 2:1 Mt/SA as affected by equilibrium solution temperature under initial concentration of 1500 mg L^{-1}.

(Fig. 2). In a similar fashion, TC adsorption at low pH on the acidic Mt clay occurred through proton uptake and the TC adsorption mechanisms were explained by cation exchange and surface complexation (Figueroa et al., 2004).

3.3. Impact of solution pH on TC adsorption

Because of TC having different forms (Fig. S1b), the pH of the solution was a pivotal factor in water treatment. In addition, the composite beads collapsed at pH >8. Therefore, the solution pH for TC adsorption was set from pH 2 to 7 (Fig. 4). The adsorption capacities were 395, 337, and 400 mg g^{-1} at pH 3 (Fig. 4) corresponding to 400, 333, and 400 mg g^{-1} at pH 3.2 (Fig. 2) for 2:1, 1:1 and original at the initial TC concentration of 1500 mg L^{-1}, respectively. For the original Mt, the trend of adsorption amounts of TC was similar as reported in previous studies (Figueroa et al., 2004; Li et al., 2005; Parolo et al., 2012; Chang et al., 2019; Zhang et al., 2019b). Moreover, the decrease of adsorption amounts with increasing pH (Fig. 3), displayed the efficiency of Mt on TC adsorption, which was mainly dependent upon the charged forms of TC (Parolo et al., 2012). In contrast, the adsorption amounts increased with increasing pH for 2:1–1:1- beads (Fig. 3). Meanwhile, the amounts of adsorption increased with increasing pH for SA. Significantly, the higher amounts of adsorption of TC on 2:1–1:1- beads were due to SA at pH 4–7. Since the SA molecule has a large number of −OH, the adsorption capacity was contributed to electrostatic interaction between the −OH of the SA and cations such as Ca^{2+} of Mt, and this behavior was also identified in the 3.2 section. Moreover, since we confirmed the filling of TC into the pore structure was not the main factor underlying enhanced adsorption, and it was monolayer adsorption, therefore, the efficiency of SA on TC adsorption under variable solution pH suggested that pore filling was not the prime reason for TC adsorption. In addition, we exclude the precipitation of TC at pH 1.5–8.7 by virtues of the results of previous study (Chang et al., 2014). The SA played an important role in the upliftment of adsorption when TC existed in a zwitteronic form at pH 3.3–7.0 (Figueroa et al., 2004) (Fig. 3). Furthermore, the crosslinking of Mt with SA introduced −OH which made the beads more hydrophobic (Kotecka and Krysinski, 2015), which was conducive to the adsorption of neutral species. TC contains several moieties that are capable of participating in H-bonding by acting as H acceptors or as both OH acceptors and H donors (hydroxyl, amide, carbonyl, and amino groups). Moreover, the gel beads are rich in oxygen-containing functional groups (hydroxyl and carboxyl groups) that strengthen hydrogen bonding under acidic solution conditions (Priya and Radha, 2017). Acidic solution can also activate the electron-acceptor capabilities of TC (Gao et al., 2012). Therefore, PVA-CA gel beads are more likely to promote π electron-donor interactions such as n-π EDA interactions, cation-π bond interactions, and cation-n bond interactions (Zhang et al., 2019b).

3.4. Effect of ionic strength on gel beads adsorption

Since cation exchange and electrostatic interaction has been shown to be the key mechanism of TC adsorption on 2:1–1:1- beads, addition of a second cation in the system is expected to decrease the TC adsorption through competition effect (Hu et al., 2017; Yang et al., 2017). Indeed, the competition was significant with an increase in concentrations of Na^{+} (Fig. 5). At the highest concentration of NaCl, the TC adsorption capacity became 135 mg g^{-1} from 400 mg g^{-1} for 2:1 bead, which likely resulted from the strong competition for adsorption sites. The influence of ionic strength for the composite beads was not significant within the concentration range of 0–0.1 mol L^{-1} of NaCl for TC (Ingerslev and Halling-Sørensen, 2000), and of 0–0.1 mol L^{-1} of NaCl for chlortetracycline (Liao et al., 2022) adsorption on gel beads compared to 0–1 mol L^{-1} NaCl in this study. However, the concentrations of Na^{+}, Ca^{2+} and Mg^{2+} were usually <100 mg L^{-1} (Liao et al., 2022), which was less than the lowest value of 0.001 mol L^{-1} NaCl in this study. Therefore, the adsorption of TC on the Mt/SA gel beads will not be influenced by co-existing cations during practical applications. TC adsorption on 2:1 and 1:1 composite beads was strongly dependent on the solution pH and ionic strength which confirmed the electrostatic attraction and cation exchange was the operative mechanisms for TC adsorption (Figueroa et al., 2004).

3.5. Effect of temperature on gel beads adsorption

The TC adsorption capacity increased with increasing temperature at an initial TC concentration of 1500 mg L^{-1} (Fig. 6), suggesting an endothermic adsorption process. The correlated equations of the underlying thermodynamics are listed below, and their parameters are shown in Table 3. Negative ΔG value obtained for original Mt in this study suggested a spontaneous adsorption process, however, the positive ΔG values for 1:1 and 2:1 Mt/SA suggested that adsorption reaction was non-spontaneous due to their relatively low positive ΔH and ΔS values as compared with original Mt (Table 3). The positive ΔH value indicated an endothermic adsorption process. The relatively positive value of ΔS, a measure of increased molecular morphology disorder, suggested the increase in system randomness as TC molecules were randomly distributed across gel bead surfaces.

Table 3
Thermodynamic parameters of TC uptake on composite beads of Mt/SA under different temperatures.

Adsorbent	pH	ln K_c			$\triangle G$ (kJ mol^{-1})			$\triangle H$ (kJ mol^{-1})	$\triangle S$ (kJ (mol K)$^{-1}$)
		298 K	313 K	328 K	298 K	313 K	328 K		
Original Mt	3–4	0.230	0.576	0.950	−0.546	−1.554	−2.562	19.483	0.067
1:1 Mt/SA	3–4	−0.948	−0.570	−0.254	2.338	1.508	0.678	18.831	0.055
2:1 Mt/SA	3–4	−0.713	−0.521	−0.392	1.687	1.373	1.060	7.924	0.021

The thermodynamic parameters of TC adsorption were deduced from the variation in where the equilibrium constant (K_c) with temperature using Eq. 1–3 (Edet and Ifelebuegu, 2020):

$$\Delta G = -RT \bullet lnK_c \quad (1)$$

$$\Delta G = \Delta H - T\Delta S \quad (2)$$

$$lnK_c = \Delta H/RT - \Delta S/R \quad (3)$$

where, thermodynamic parameters T is the temperature (K), R is the universal gas constant (8.314 J (mol•K)$^{-1}$), ΔH is the enthalpy change (kJ mol^{-1}), ΔS is the entropy change (kJ (mol•K)$^{-1}$), and the free energy of adsorption ΔG (kJ mol^{-1}). The K_c is the C_a/C_e. The C_a is the amount of adsorbate adsorbed at equilibrium (mg L^{-1}) and C_e is the concentration of the adsorbate in the solution at equilibrium (mg L^{-1}), respectively.

3.6. Derivative thermogravimetric (DTG) analyses

For the powder Mt, the thermogravimetric (TG) and derivative of TG (DTG) exhibited a decomposition temperature (T_{peak}) at 60 °C with a mass loss of 18%, which was attributed to the removal of adsorbed water, and a subsequent T_{peak} at 155 °C attributed to interlayer water loss (Guggenheim and Groos, 2001) (Fig. 7a, b). When the amount of intercalated TC was 0.77 CEC, the T_{peak} at 155 °C disappeared, indicating the absence of interlayer water. The total mass loss of adsorbed and interlayer waters was about 20% for the original Mt, which gradually decreased to 7 and 3% as the CEC increased from 0.59 to 0.77 (Fig. 7a). This indicated that TC replaced water in the interlayers. The progressive increase in total mass loss from 0.59 to 0.77 CEC confirmed the presence of TC either on the surface or in the interlayer of the original Mt (Fig. 7a). In comparison, TC by itself exhibited 20% to 80% of mass loss with a T_{peak} at 260 °C to a T_{peak} at 570 °C (Fig. 7b). The increase in TC T_{peak} to 310 °C, 620 °C, and 700 °C after adsorption (Fig. 7a) was attributed to TC-clay intercalation (Chang et al., 2014).

For 1:1 Mt/SA (Fig. 7c, d), the cations accompanied with two water molecule layers in the interlayers of Mt, has been shown to exist by ion chromatography (IC) according to the form of gel beads. Thus, the T_{peak} at 60 °C and 155 °C of adsorbed water and interlayer water, respectively, should appear in 1:1 Mt/SA (Fig. 7c, d), but they disappeared. This might be due to the protection of the SA structure that rendered this T_{peak} to enhance to T_{peak} at 210 °C, as their mass loss was almost close to 0 (Fig. 7c). The T_{peak} of SA at 270 °C was the degradation temperature (Kragović et al., 2016) which decreased to 210 °C. Furthermore, the peak of adsorbed water appeared again for 0.59 and 0.89 CEC of the adsorbed samples and combined to a broad peak at T_{peak} at 60 °C (Fig. 7a). This T_{peak} of TC at 260 °C and 570 °C increased to 290 °C and 710 °C (Fig. 7d), and this increasing trend also appeared for 2:1 Mt/SA adsorbed samples (Fig. 7f). Besides, the total mass loss of 1:1 Mt/SA and 2:1 Mt/SA were almost the same (Fig. 7c, e). The T_{peak} of SA at 570 °C belonged to the decomposition temperature (Kragović et al., 2016). It was difficult to justify the T_{peak} of adsorbed samples at 710° as owing to TC or SA because both of them have the same T_{peak} at 570 °C (Fig. 7d), but these T_{peaks} all shifted to a higher temperature (Fig. 7d, f) and confirmed the enhancement of T_{peak} of TC or SA for adsorbed samples.

3.7. XRD analysis of the Mt/SA beads

Since cation exchange was shown to be the main adsorption mechanism, many studies have shown that the d-value of Mt changed after the adsorption of organic compounds (Hao et al., 2021). Because physical grinding is not able to destroy chemical bonds, the raw gel beads and adsorption samples were carefully ground to form powders for XRD analysis (Fig. 8a, b, c). The XRD patterns of the original, 2:1- and 1:1-beads remained almost similar (inserted figure in Fig. 8a), which indicated that SA was not inserted into the Mt interlayers. The results showed the 001 reflection for the raw Mt at 5.74° (2θ) (Fig. 8a), which corresponded to a d-value of 15.4 Å and indicated that the interlayer cation was Ca^{2+} with two layers of water associated for hydration (Chang et al., 2014). After addition of the TC with different initial concentrations, the 001 reflection became broader and reached a plateau at 0.12 and 0.29 cation exchange capacity (CEC), respectively. This plateau indicated that SAz-2 was a mixed-layered clay composed of pure SAz-2 and SAz-2 intercalated with TC at this adsorption level (Chang et al., 2014). Since the amount of TC intercalated was higher than 0.46 CEC, an obvious shift in the 001 reflection to a lower angle and a large increase in the full width at half maximum (FWHM) was observed, and the basal spacing expanded to 21.03 Å. At 0.77 CEC, the basal spacing of the 001 reflection increased to 21.20 Å (Fig. 8a). Again, the large FWHM showed that the crystallinity of the SAz-2 was much lower after intercalation of the TC. Furthermore, 002 reflections appeared at adsorption levels of 0.46–0.77 CEC, which was never found for raw Mt (insert figure in Fig. 8a); this suggested a disordered transition of the SAz-1 structure and larger amounts of TC intercalated (Chang et al., 2009a). Meanwhile, the d-value of the 002 reflection was 10.52 Å, almost half of 21.03 Å, which corresponded to the mineral characterization via XRD.

The variations in the d-values for the 2:1- and 1:1-beads were the same as those of the original Mt (Fig. 8b, c). They were presented as transitions involving the formation of mechanical mixtures, materials of intermediate layer thicknesses, and/or mixed layering of different ordered states during the intercalation process. In particular, the intensities of the 002 reflections were larger than those of the original Mt, again suggesting that there was more adsorption on the 2:1- and 1:1-beads. Additionally, the 001 and 002 reflections showed regular appearances. In addition, the d-value was increased to 21.37 Å, which exceeded 21.20 Å, and this supported the higher amounts adsorbed by the 2:1- and 1:1-beads (Fig. 8b, c).

Overall, for all samples adsorbed on the 2:1- and 1:1-beads, the trend for order-disorder of the 00 l reflections indicated transitions from practically perfect situations of mixed-layer ordering to relatively low degrees of ordering for the low-to-intermediate levels of intercalation, and high levels of intercalation returned to a perfect ordering situation. In addition, the consistencies of these reflections locations and intensities strongly suggested that adsorption of TC occurred on the internal surfaces of the Mt (Fig. 8a).

3.8. FTIR analyses

For isotherm studies, the FTIR spectra of the samples with different CEC values are illustrated in Fig. 9a, b, c, and the characteristic positions are listed in Table S4. The characteristic bands for TC are those at 1200–1800 cm^{-1}. Overall, the vibrational bands for the crystalline TC

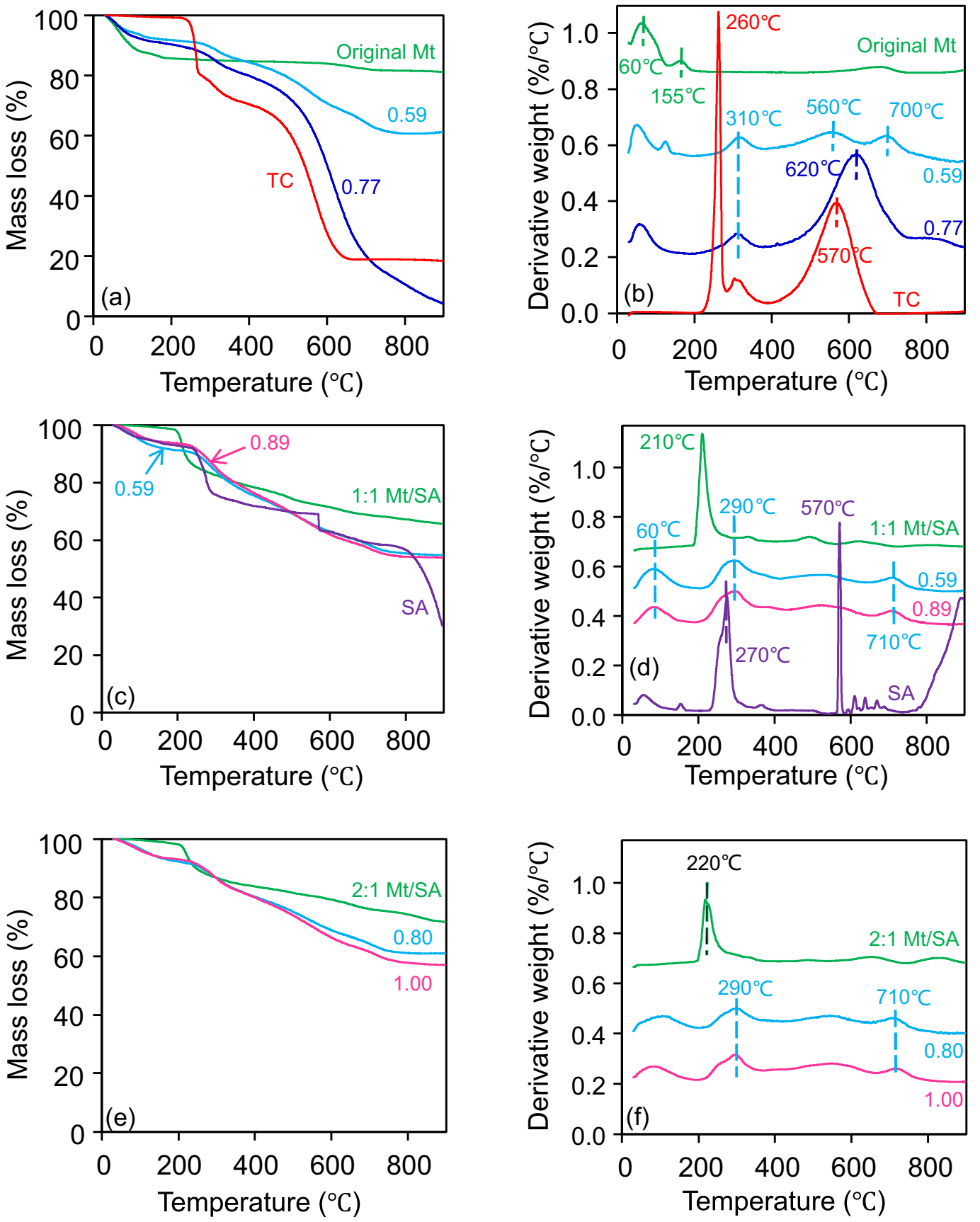

Fig. 7. TGA (a) and DTG (b) analyses of original Mt, TC, SA and original Mt equilibrated with different amounts of TC. TGA (c) and DTG (d) analyses of 1:1 Mt/SA, TC, SA and 1:1 Mt/SA equilibrated with different amounts of TC. TGA (e) and DTG (f) analyses of 2:1 Mt/SA, TC, SA and 2:1 Mt/SA equilibrated with different CEC values of TC.

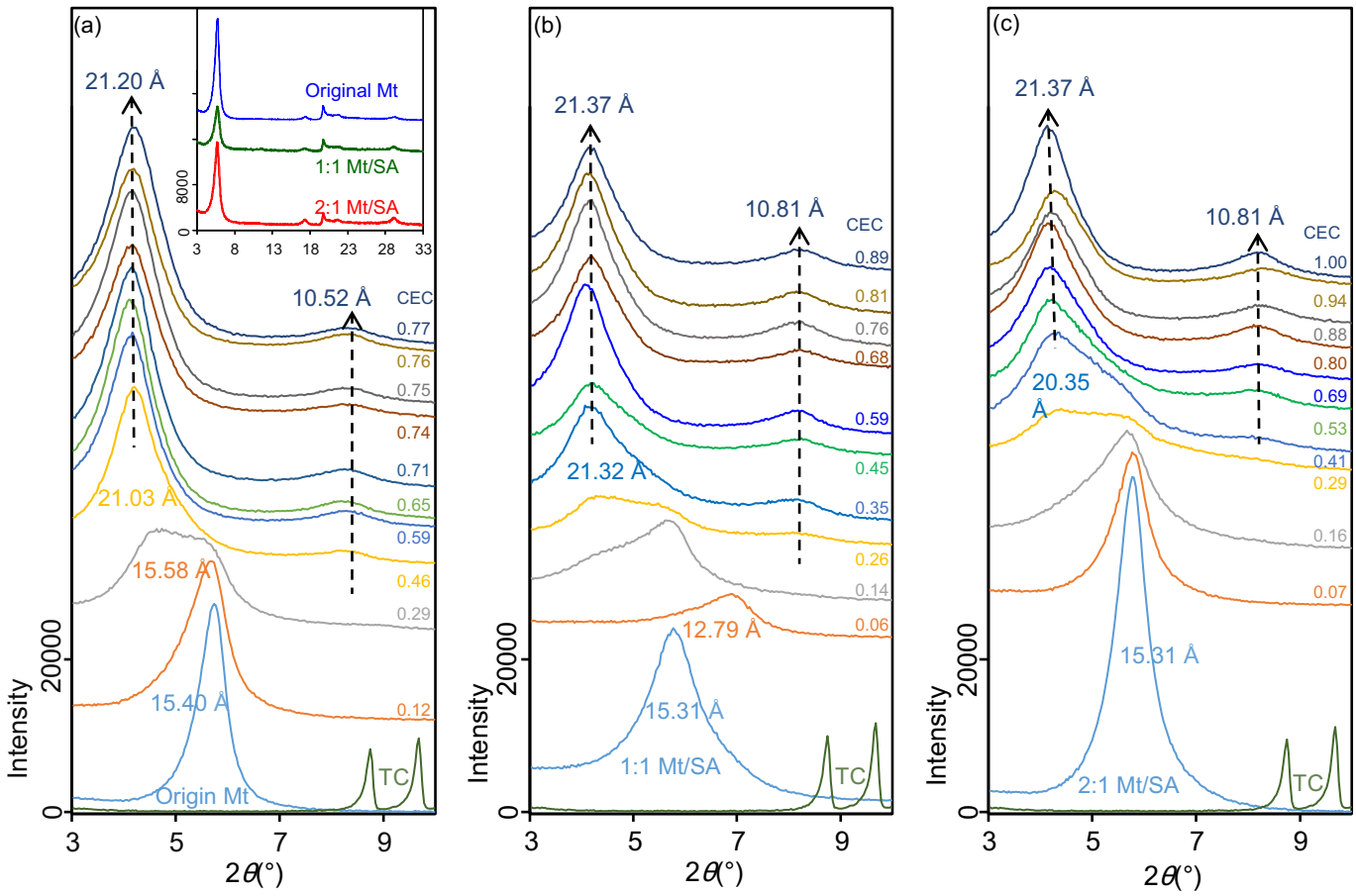

Fig. 8. XRD patterns of TC-adsorbed original Mt (a),1:1 Mt/SA (b), and 2:1 Mt/SA (c) with different adsorption amounts as CEC values of TC.

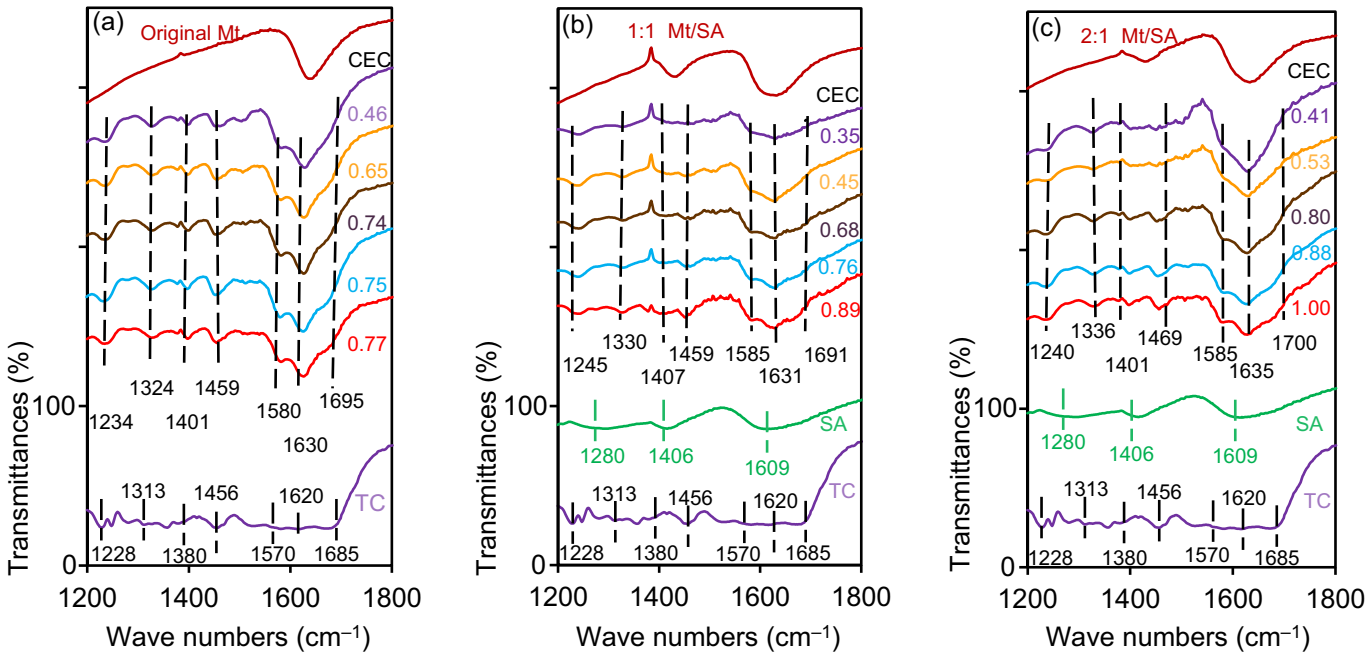

Fig. 9. FTIR spectra of TC-adsorbed original Mt (a), 1:1 Mt/SA (b), and 2:1 Mt/SA (c) with different amounts with CEC values of TC in the wavenumber ranges of 1200–1800 cm^{-1}.

matched well with previously reported data (Priya and Radha, 2017). The bands at 1616 and 1578 cm^{-1} corresponded to the carbonyl groups in the A and C rings, respectively, while the 1455 cm^{-1} band was assigned to a skeletal vibration (Schlecht et al., 1974). They were all shifted to higher frequencies (Fig. 9; Table S4) (Gu and Karthikeyan, 2005; Leypold et al., 2003), in contrast to the shifts to lower frequencies

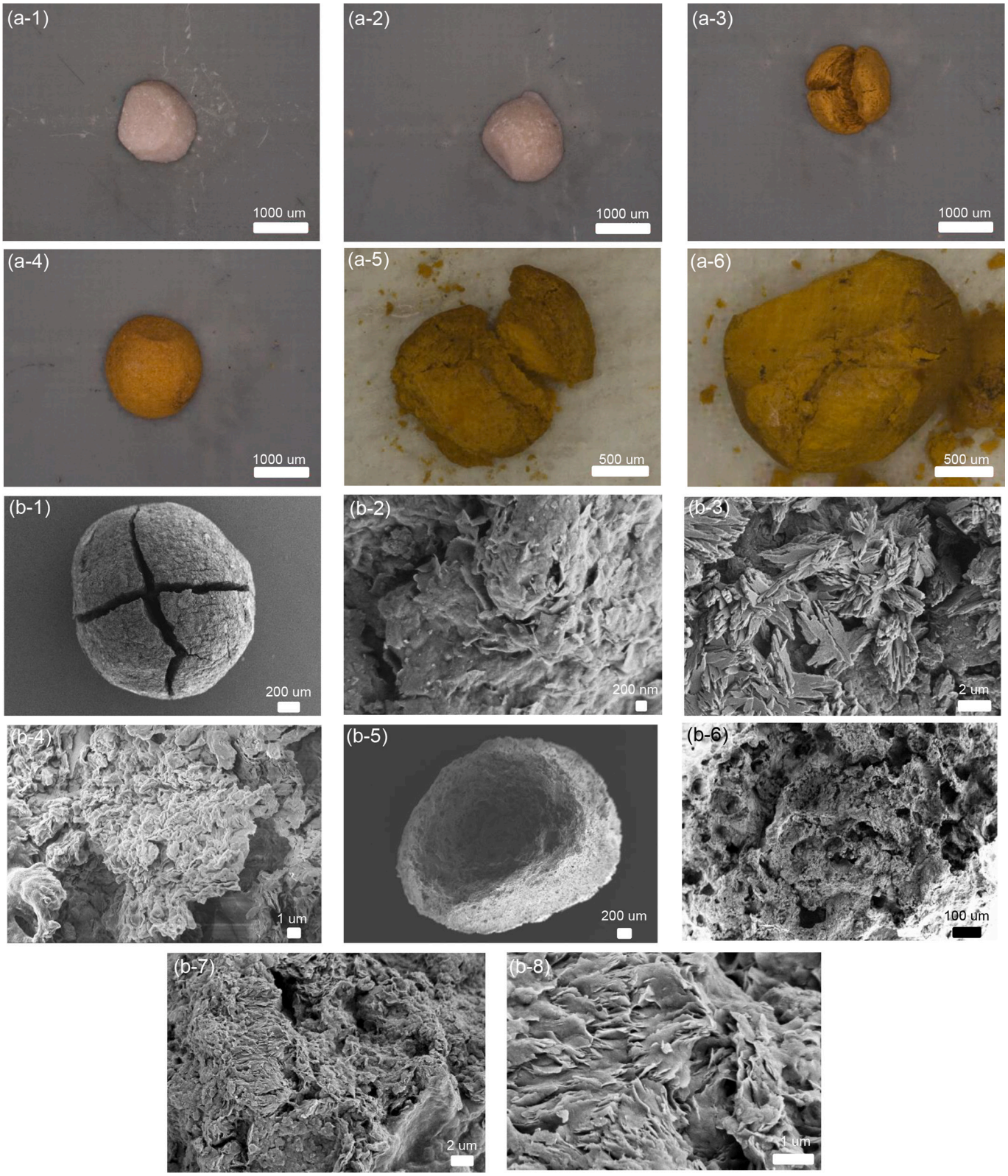

Fig. 10. Visible images (a-1–6) of 1:1 Mt/SA (a-1), 2:1 Mt/SA (a-2), and after in contact TC with 4000 mg L^{-1} (a-3, 4), and their profile images (a-5, 6), respectively. SEM images (b-1–8) of 1:1 Mt/SA (b-1), 2:1 Mt/SA (b-5). And, their structures for 1:1 Mt/SA (b-2, b-3, b-4) and 2:1 Mt/SA (b-6, b-7, b-8) under different magnifications.

reported for Mt (Caminati et al., 2002; Porubcan et al., 1978). Shifts to higher frequencies resulted from a strong interaction between the Mt surface and the intercalated TC (Kim et al., 2013), which suggested that the amide functional group participated in TC intercalation. The other peaks, present at 1227 cm^{-1} (Schlecht et al., 1974) and 1675 cm^{-1} (Kulshrestha et al., 2004), confirmed that the amide group was involved in adsorption. Furthermore, the peak positions for raw SA, 1:1 Mt/SA, and 2:1 Mt/SA are shown in Table S5. The shifts indicated the existence of (COO^-) and ($CH–OCH_2$) moieties in the SA, which indicated that the interactions between the SA and oxides on the Mt surface involved the formation of H-bonds (Gambinossi et al., 2004). Participation of the amine and dimethylamino groups in TC required a horizontal orientation on the internal surfaces of the 2:1 and 1:1 composite beads, as confirmed by the XRD and FTIR results.

3.9. Laser microscopy and FE-SEM images

The laser microscopy images (Fig. 10), such as those for the colorful TC adsorbate, showed that the composite beads (Fig. 10a-1, −2) were full of the yellowish TC (Fig. 10a-3, −4) or their profile (Fig. 10a-5, −6) at the initial concentration of 1500 mg L^{-1}, indicated that these composite beads made of Mt adsorbed ample TC even inside the beads. On the other hand, some of the composite beads obtained after oven-drying were full of fractures (Fig. 10a-3), and some of them showed a smooth surface morphology (Fig. 10a-4). Nevertheless, these beads were stable and did not collapse at pH between 2 and 7.

The FE-SEM images indicated that the composite beads were full of pores (Fig. 10b-1, −2, −4, −5, −6, −7). Furthermore, the layered structure of Mt was still visible after granulation with the SA (Fig. 10b-3, −8). These structures indicated the possibility of cation exchange between the Mt and TC. These micron-scale pores provided pathways for entry of the nanosized TC molecules into the interiors of the beads and enhanced the adsorption capacities of the 2:1- and 1:1-Mt/SA beads.

3.10. Adsorption mechanism

We identified electrostatic attraction between the −OH of SA and the cationic TC as one of the main adsorption mechanisms operating at low solution pH (Fig. S6). In addition, several previous studies described the adsorption mechanism between TC and composite beads made of Mt/SA, and these included combinations of H-bonding, cation-n pair bonding interactions, cation-π bond interactions, and n-π EDA interactions (Zhang et al., 2019b). The multiple mechanisms for TC adsorption were shown to include hydrophobic interactions, n-π EDA interactions, cation bonding bridges, electrostatic interactions, and hydrogen bonding (Farea et al., 2020; Liao et al., 2022). However, in this study, we investigated the capacity for TC adsorption on the pure SA beads and confirmed the adsorption capacities of the 2:1- and 1:1-beads. Moreover, the desorbed cations confirmed that cation exchange was one of the main adsorption mechanisms that increased the adsorption capacity potential up to 745 and 689 mg g^{-1} for the 2:1- and 1:1-beads, respectively. Many previous studies indicated that large adsorption capacities for powdered Mt clay were always caused by cation exchange phenomenon (Chang et al., 2019; Figueroa et al., 2004). Moreover, the d-value for Mt in the 2:1- and 1:1-beads increased with increasing adsorption capacity, and the increased decomposition temperature for TC indicated intercalation (Chang et al., 2019). Under these scenarios, cation exchange between the Mt and TC was the main adsorption mechanism, and H-bonding between the SA and TC was also involved in the adsorption processes of the 2:1- and 1:1-beads (Fig. S6).

4. Conclusions and future research direction

In this study, novel Mt/SA composite beads were successfully prepared using 2:1 and 1:1 Mt/SA ratios and evaluated for the removal of TC antibiotic from aqueous system. The XRD, FTIR, FE-SEM and laser microscopy analyses revealed that Mt/SA composite beads were porous and had significantly different physicochemical and morphological properties than raw Mt. The 2:1 Mt/SA exhibited excellent TC adsorption capacity of 745 mg g^{-1} compared to raw Mt (445 mg g^{-1}) and reached equilibrium within 8 h. Cation exchange was proved as the principal mechanism for TC adsorption. The Mt/SA beads were successful to remove TC under pH 2–7. The significance of the study lies in the successful formulation of beads from Mt/SA composites that provided an excellent TC adsorption capacity making the separation of the beads quite easier from aqueous solution compared to a powdered adsorbent. Overall, this study provides a novel, inexpensive and green approach to remove TC from aqueous system. The stability of beads under a wide range of pH, assessment of TC removal performance from real wastewater and evaluation of ecotoxicological impacts of the beads, if any, require future research attention.

Author statement

PC: Conceptualization, experimental design and preparation of the first draft of the manuscript. PC and RM: Data checking, analyses. RM and BS: Results interpretation and improvement of the manuscript. YM and CH: Experiments and instrumental analysis. PC and YT: Funding acquisition and supervision.

Declaration of Competing Interest

The authors declare that they have no known competing financial interests or personal relationships that could have appeared to influence the work reported in this paper.

Data availability

Data will be made available on request.

Acknowledgments

The authors are grateful to the Ministry of Science and Technology, Republic of China (ROC), under project numbers 109-2811-B-005-505 and 110-2313-B-005-023-MY3 for financial support to Po-Hsiang Chang and Yu-Min Tzou. This work was financially supported by the “Innovation and Development Center of Sustainable Agriculture” from The Featured Areas Research Center Program within the framework of the Higher Education Sprout Project by the Ministry of Education (MOE) in Taiwan. The acquisition of Fig. S6 and some raw figures by Jiwei Li of Xi’an Jiaotong University is highly appreciated.

Appendix A. Supplementary data

Supplementary data to this article can be found online at https://doi.org/10.1016/j.clay.2023.107127.

References

Aristilde, L., Lanson, B., Miéhé-Brendlé, J., Marichal, C., Charlet, L., 2016. Enhanced interlayer trapping of a tetracycline antibiotic within montmorillonite layers in the presence of Ca and Mg. J. Colloid Interface Sci. 464, 153–159. https://doi.org/10.1016/j.jcis.2015.11.027.

Ashraf, A., Liu, G., Arif, M., Mian, M.M., Rashid, A., Yousaf, B., Khawar, M.I., Riaz, L., Safeer, R., 2022. Insights into the synthesis and application of biochar assisted graphene-based materials in antibiotic remediation. J. Clean. Prod. 361, 132211 https://doi.org/10.1016/j.jclepro.2022.132211.

Azanu, D., Styrishave, B., Darko, G., Weisser, J.J., Abaidoo, R.C., 2018. Occurrence and risk assessment of antibiotics in water and lettuce in Ghana. Sci. Total Environ. 622–623, 293–305. https://doi.org/10.1016/j.scitotenv.2017.11.287.

Benavides, S., Carvajal, R.V., Reyes, J.E., 2012. Physical, mechanical and antibacterial properties of alginate film: effect of the crosslinking degree and oregano essential oil concentration. J. Food Eng. 110, 232–239. https://doi.org/10.1016/j.jfoodeng.2011.05.023.

Caminati, G., Focardi, C., Gabrielli, G., Gambinossi, F., Mecheri, B., Nocentini, M., Puggelli, M., 2002. Spectroscopic investigation of tetracycline interaction with

phospholipid Langmuir-Blodgett films. Mater. Sci. Eng. C 22, 301–305. https://doi.org/10.1016/S0928-4931(02)00217-5.
Chang, P.-H., Li, Z., Jiang, W.-T., Jean, J.-S., 2009a. Adsorption and intercalation of tetracycline by swelling clay minerals. Appl. Clay Sci. 46, 27–36. https://doi.org/10.1016/j.clay.2009.07.002.
Chang, P.-H., Jean, J.-S., Jiang, W.-T., Li, Z., 2009b. Mechanism of tetracycline sorption on rectorite. Colloids Surf. A - Physicochem. Eng. Asp. 339, 94–99. https://doi.org/10.1016/j.colsurfa.2009.02.002.
Chang, P.-H., Li, Z., Jiang, W.-T., Kuo, C.-Y., Jean, J.-S., 2014. Adsorption of tetracycline on montmorillonite: influence of solution pH, temperature, and ionic strength. Desalin. Water Treat. 55, 1380–1392. https://doi.org/10.1080/19443994.2014.924881.
Chang, P.-H., Sarkar, B., Jiang, W.-T., Li, Z., 2019. Clay minerals for pharmaceutical wastewater treatment. In: Mercurio, M., Sarkar, B., Langella, A. (Eds.), Modifed Clay and Zeolite Nanocomposites Materials. Elsevier, Amsterdam, pp. 167–196. https://doi.org/10.1016/B978-0-12-814617-0.00011-6.
Daghrir, R., Drogui, P., 2013. Tetracycline antibiotics in the environment: a review. Environ. Chem. Lett. 11, 209–227. https://doi.org/10.1007/s10311-013-0404-8.
Das, T.K., Scott, Q., Bezbaruah, A.N., 2021. Montmorillonite-iron crosslinked alginate beads for aqueous phosphate removal. Chemosphere 281, 130837. https://doi.org/10.1016/j.chemosphere.2021.130837.
Edet, U.A., Ifelebuegu, A.O., 2020. Kinetics, isotherms, and thermodynamic modelling of the adsorption of phosphates from model wastewater using recycled brick waste. Processes 8, 665. https://doi.org/10.3390/pr8060665.
Farea, M.O., Abdelghany, A.M., Oraby, A.H., 2020. Optical and dielectric characteristics of polyethylene oxide/sodium alginate-modified gold nanocomposites. RSC Adv. 10, 37621–37630. https://doi.org/10.1039/D0RA07601E.
Fernandes, R.D., Moura, M.R.D., Glenn, G.M., Aouada, F.A., 2018. Thermal, microstructural, and spectroscopic analysis of Ca^{2+} alginate/clay nanocomposite hydrogel beads. J. Mol. Liq. 265, 327–336. https://doi.org/10.1016/j.molliq.2018.06.005.
Figueroa, R.A., Leonard, A., MacKay, A.A., 2004. Modeling tetracycline antibiotic sorption to clays. Environ. Sci. Technol. 3, 476–483. https://doi.org/10.1021/es0342087.
Gambinossi, F., Mecheri, B., Nocentini, M., Puggelli, M., Caminati, G., 2004. Effect of the phospholipid head group in antibiotic-phospholipid association at water-air interface. Biophys. Chem. 110, 101–117. https://doi.org/10.1016/j.bpc.2004.01.008.
Gao, X., Zhang, Y., Zhao, Y., 2018. Zinc oxide templating of porous alginate beads for the recovery of gold ions. Carbohydr. Polym. 200, 297–304. https://doi.org/10.1016/j.carbpol.2018.07.097.
Gao, X., Li, M., Zhao, Y., 2019. Mechanistic study of selective adsorption of Hg^{2+} ion by porous alginate beads. Chem. Eng. J. 378, 122096 https://doi.org/10.1016/j.cej.2019.122096.
Gao, Y., Li, Y., Zhang, L., Huang, H., Hu, J., Shah, S.M., Su, X., 2012. Adsorption and removal of tetracycline antibiotics from aqueous solution by graphene oxide. J. Colloid Interface Sci. 368, 540–546. https://doi.org/10.1016/j.jcis.2011.11.015.
Gu, C., Karthikeyan, K.G., 2005. Interaction of tetracycline with aluminum and iron hydrous oxides. Environ. Sci. Technol. 39, 2660–2667. https://doi.org/10.1021/es048603o.
Guggenheim, S., Groos, A.F.K., 2001. Baseline studies of the clay minerals society source clays: thermal analysis. Clay Clay Miner. 49, 433–443. https://doi.org/10.1346/CCMN.2001.0490509.
Hao, D., Chen, Y., Zhang, Y., You, N., 2021. Nanocomposites of zero-valent iron@biochar derived from agricultural wastes for adsorptive removal of tetracyclines. Chemosphere 284, 131342. https://doi.org/10.1016/j.chemosphere.2021.131342.
He, J., Ni, F., Cui, A., Chen, X., Deng, S., Shen, F., Huang, C., Yang, G., Song, C., Zhang, J., Tian, D., Long, L., Zhu, Y., Luo, L., 2020. New insight into adsorption and co-adsorption of arsenic and tetracycline using a Y-immobilized graphene oxide-alginate hydrogel: Adsorption behaviours and mechanisms. Sci. Total Environ. 701, 134363 https://doi.org/10.1016/j.scitotenv.2019.134363.
Hou, D., Gui, R., Hu, S., Huang, Y., Feng, Z., Ping, Q., 2015. Preparation and characterization of novel drug-inserted-montmorillonite chitosan carriers for ocular drug delivery. Adv. Nanopart. 4, 70–84. https://doi.org/10.4236/anp.2015.43009.
Hu, A., Yang, X., You, Q., Liu, Y., Wang, Q., Liao, G., Wang, D., 2019. Magnetically hyper-cross-linked polymers with well-developed mesoporous: a broad-spectrum and highly efficient adsorbent for water purification. J. Mater. Sci. 54, 2712–2728. https://doi.org/10.1007/s10853-018-2967-z.
Hu, X.J., Zhao, Y.L., Wang, H., Tan, X.F., Yang, Y.X., Liu, Y.G., 2017. Efficient removal of tetracycline from aqueous media with a Fe3O4 nanoparticles@graphene oxide nanosheets assembly. Int. J. Environ. Res. Public Health 14, 1495–1509. https://doi.org/10.3390/ijerph14121495.
Hu, Z.-T., Wang, X.-F., Xiang, S., Ding, Y., Zhao, D.Y., Hu, M., Pan, Z., Varjani, S., Wong, J.W.C., Zhao, J., 2022. Self-cleaning Mn-Zn ferrite/biochar adsorbents for effective removal of tetracycline. Sci. Total Environ. 844, 157202 https://doi.org/10.1016/j.scitotenv.2022.157202.
Huang, D., Wu, J.Z., Wang, L., Liu, X.M., Meng, J., Tang, X.J., Tang, C.X., Xu, J.M., 2019. Novel insight into adsorption and co-adsorption of heavy metal ions and an organic pollutant by magnetic graphene nanomaterials in water. Chem. Eng. J. 358, 1399–1409. https://doi.org/10.1016/j.cej.2018.10.138.
Ingerslev, F., Halling-Sørensen, B., 2000. Biodegradability properties of sulfonamides in activated sludge. Environ. Toxicol. Chem. 19, 2467–2473. https://doi.org/10.1002/etc.5620191011.
Kim, E.J., Lee, C.S., Chang, Y.Y., Chang, Y.S., 2013. Hierarchically structured manganese oxide-coated magnetic nanocomposites for the efficient removal of heavy metal ions from aqueous systems. ACS Appl. Mater. Interfaces 5, 9628–9634. https://doi.org/10.1021/am402615m.
Kotecka, K., Krysinski, P., 2015. Effect of tetracycline antibiotic on the monolayers of phosphatidylcholines at the air–water interface. Colloids Surf. A Physicochem. Eng. Asp. 482, 678–686. https://doi.org/10.1016/j.colsurfa.2015.05.055.
Kragović, M., Daković, A., Marković, M., Petković, A., 2016. Kinetic of thermal degradation of alginate-zeolite composites. Zastita Materijala 57, 559–564. https://doi.org/10.5937/ZasMat1604559K.
Kulshrestha, P., Giese, R.F., Aga, D.S., 2004. Investigating the molecular interactions of oxytetracycline in clay and organic matter: insights on factors affecting its mobility in soil. Environ. Sci. Technol. 38, 4097–4105. https://doi.org/10.1021/es034856q.
Leypold, C.F., Reiher, M., Brehm, G., Schmitt, M.O., Schneider, S., Matousek, P., Towrie, M., 2003. Tetracycline and derivatives-assignment of IR and Raman spectra via DFT calculations. Phys. Chem. Chem. Phys. 5, 1149–1157. https://doi.org/10.1039/B210522E.
Li, B., Zhang, T., 2010. Biodegradation and adsorption of antibiotics in the activated sludge process. Environ. Sci. Technol. 44, 3468–3473. https://doi.org/10.1021/es903490h.
Li, J., Zhang, H., Chen, Y., Luo, Y., Zhang, H., 2016. Sources identification of antibiotic pollution combining land use information and multivariate statistics. Environ. Monit. Assess. 188, 430. https://doi.org/10.1007/s10661-016-5439-4.
Li, Z., Ramay, H.R., Hauch, K.D., Xiao, D., Zhang, M., 2005. Chitosan-alginate hybrid scaffolds for bone tissue engineering. Biomaterials 261, 3919–3928. https://doi.org/10.1016/j.biomaterials.2004.09.062.
Liang, B., Zhao, H., Zhang, Q., Fan, Y., Yue, Y., Yin, P., Guo, L., 2016. Ca^{2+} enhanced nacre-inspired montmorillonite-alginate film with superior mechanical, transparent, fire retardancy, and shape memory properties. ACS Appl. Mater. Interfaces 8, 28816–28823. https://doi.org/10.1021/acsami.6b08203.
Liao, J.F., Wang, B.Y., Huang, Y.X., Qu, Y., Peng, J.R., Qian, Z.Y., 2017. Injectable alginate hydrogel cross-linked by calcium gluconate-loaded porous microspheres for cartilage tissue engineering. ACS Omega 2, 443–454. https://doi.org/10.1021/acsomega.6b00495.
Liao, Q., Rong, H., Zhao, M., Luo, H., Chu, Z., Wang, R., 2022. Strong adsorption properties and mechanism of action with regard to tetracycline adsorption of double-network polyvinyl alcohol-copper alginate gel beads. J. Hazard. Mater. 422, 126863 https://doi.org/10.1016/j.jhazmat.2021.126863.
Mohammed, A., Rivers, A., Stuckey, D.C., Ward, K., 2020. Alginate extraction from Sargassum seaweed in the Caribbean region:optimization using response surface methodology. Carbohydr. Polym. 245, 116419 https://doi.org/10.1016/j.carbpol.2020.116419.
Park, J.H., Shin, H.J., Kim, M.H., Kim, J.S., Kang, N., Lee, J.Y., Kim, K.T., Lee, J.I., Kim, D.D., 2016. Application of montmorillonite in bentonite as a pharmaceutical excipient in drug delivery systems. J. Pharm. Investig. 46, 363–375. https://doi.org/10.1007/s40005-016-0258-8.
Parolo, M.E., Avena, M.J., Pettinari, G.R., Baschini, M.T., 2012. Influence of Ca^{2+} on tetracycline adsorption on montmorillonite. J. Colloid Interface Sci. 368, 420–426. https://doi.org/10.1016/j.jcis.2011.10.079.
Peng, H., Wang, H., Wang, L., Huang, C., Zheng, X., Wen, J., 2022. Efficient adsorption-photocatalytic removal of tetracycline hydrochloride over La_2S_3-modified biochar with S, N-codoping. J. Water Proc. Eng. 49, 103038 https://doi.org/10.3390/ijms23169343.
Porubcan, L.S., Serna, C.J., White, J.L., Hem, S.L., 1978. Mechanism of adsorption of clindamycin and tetracycline by montmorillonite. J. Pharm. Sci. 67, 1081–1087. https://doi.org/10.1002/jps.2600670815.
Priya, S.S., Radha, K.V., 2017. A review on the adsorption studies of tetracycline onto various types of adsorbents. Chem. Eng. Commun. 204, 821–839. https://doi.org/10.1080/00986445.2015.1065820.
Roberts, M.C., 2002. Resistance to tetracycline, macrolide-lincosamide-streptogramin, trimethoprim, and sulfonamide drug classes. Mol. Biotechnol. 20, 261–283. https://doi.org/10.1385/MB:20:3:261.
Sarmah, A.K., Meyer, M.T., Boxall, A.B.A., 2006. A global perspective on the use, sales, exposure pathways, occurrence, fate and effects of veterinary antibiotics (VAs) in the environment. Chemosphere 65, 725–759. https://doi.org/10.1016/j.chemosphere.2006.03.026.
Schlecht, K.D., Dix, R.B., Tamul, M.J., 1974. Internal reflection spectra of several tetracyclines. Appl. Spectrosc. 28, 38–40. https://doi.org/10.1366/000370274774332984.
Tong, L., Li, P., Wang, Y., Zhu, K., 2009. Analysis of veterinary antibiotic residues in swine wastewater and environmental water samples using optimized SPE-LC/MS/MS. Chemosphere 74, 1090–1097. https://doi.org/10.1016/j.chemosphere.2008.10.051.
Yan, C., Yi, Y., Zhou, J., Liu, M., Nie, M., Shi, H., Gu, L., 2013. Antibiotics in the surface water of the Yangtze Estuary: Occurrence, distribution and risk assessment. Environ. Pollut. 175, 22–29. https://doi.org/10.1016/j.envpol.2012.12.008.
Yang, Y.X., Hu, X.J., Zhao, Y.L., Cui, L.H., Huang, Z.J., Long, J.L., Xu, J.W., Deng, J.B., Wu, C.Y., Liao, W.W., 2017. Decontamination of tetracycline by thiourea-dioxide-reduced magnetic graphene oxide: effects of pH, ionic strength, and humic acid concentration. J. Colloid Interface Sci. 495, 68–77. https://doi.org/10.1016/j.jcis.2017.01.075.
You, N., Chen, S., Wang, Y., Fan, H.-T., Sun, L.-N., Sun, T., 2020. In situ sampling of tetracycline antibiotics in culture wastewater using diffusive gradients in thin films equipped with graphene nanoplatelets. Environ. Res. 191, 110089 https://doi.org/10.1016/j.envres.2020.110089.
Yu, F., Li, Y., Han, S., Ma, J., 2016. Adsorptive removal of antibiotics from aqueous solution using carbon materials. Chemosphere 153, 365–385. https://doi.org/10.1016/j.chemosphere.2016.03.083.

Zhang, H., Chu, L., Wang, J., Guo, Q., Zhang, W., 2023. Iron/nickel decorated palygorskite-sodium alginate beads for tetracycline removal. Chem. Eng. Res. Design 190, 106–116. https://doi.org/10.1016/j.cherd.2022.11.053.

Zhang, X., Lin, X., He, Y., Chen, Y., Luo, X., Shang, R., 2019a. Study on adsorption of tetracycline by Cu-immobilized alginate adsorbent from water environment. Int. J. Biol. Macromol. 124, 418–428. https://doi.org/10.1016/j.ijbiomac.2018.11.218.

Zhang, X., Lin, X., He, Y., Luo, X., 2019b. Phenolic hydroxyl derived copper alginate microspheres as superior adsorbent for effective adsorption of tetracycline. Int. J. Biol. Macromol. 136, 445–459. https://doi.org/10.1016/j.ijbiomac.2019.05.165.

Zhu, Runliang, Chen, Qingze, Zhou, Qing, Xi, Yunfei, Zhu, Jianxi, He, Hongping, 2016. Adsorbents based on montmorillonite for contaminant removal from water: a review. Appl. Clay Sci. 123, 239–258. https://doi.org/10.1016/j.clay.2015.12.024.

Zou, S.-J., Chen, Y.-F., Zhang, Y., Wang, X.-F., You, N., Fan, H.-T., 2022. A hybrid sorbent of α-iron oxide/reduced graphene oxide: studies for adsorptive removal of tetracycline antibiotics. J. Alloys Compd. 863, 158475 https://doi.org/10.1016/j.jallcom.2020.158475.